VNU Journal of Science: Mathematics - Physics
Journal homepage: https://js.vnu.edu.vn/MaP

Original Article

Tunable Localized Surface Plasmon Resonance of Gold Nanorod by Control of Sodium Oleate

Pham Thi Thu Ha[1], Pham Thi Nga[1,2], Ha Phuong Lan[1,3], Lai Tong Anh Kiet[1], Nguyen Dac Dien[4], Tran Thu Trang[1], Chu Thi Hong Huyen[1], Nguyen Thi Tuyet[1], Nguyen Vu Anh Tuyet[1,5], Vu Xuan Hoa[1,*]

[1]*TNU-University of Sciences, Phan Dinh Phung, Thai Nguyen, Vietnam*

[2]*Hoa Lu University, 2 Xuan Thanh, Hoa Lu, Ninh Binh, Vietnam*

[3]*Cvi Cosmetic and Pharmaceutical Joint Stock Company, Lot CN1-08B-3, High Tech Industrial Zone 1-Hoa Lac High Tech Park, Km29 Thang Long Ave, Hoa Lac, Hanoi, Vietnam*

[4]*Vietnam Trade Union University, 169 Tay Son, Dong Da, Hanoi, Vietnam*

[5]*Hung Yen High School for the Gifted, 1 Chu Van An, Pho Hien, Hung Yen, Vietnam*

Received 2nd May 2025
Revised 26th June 2025; Accepted 22nd July 2025

Abstract: Gold nanorods (AuNRs) are powerful plasmonic nanomaterials with tunable localized surface plasmon resonance (LSPR) that make them ideal for surface-enhanced Raman scattering (SERS) sensing. In this work, we report results on a sodium oleate (NaOL)-assisted seed-mediated synthesis of AuNRs in a cetyltrimethylammonium bromide (CTAB)-based system. Varying NaOL amount allowed to control the nanorods aspect ratio, improve monodispersity. The resulting products have been checked on X-ray diffraction (XRD), ultraviolet-visible (UV-Vis) spectroscopy, transmission electron microscopy (TEM), high-resolution TEM (HRTEM), and energy-dispersive X-ray spectroscopy (EDS).

Keywords: Gold nanorods, localized surface plasmon resonance, sodium oleate, surfactant.

1. Introduction

Gold nanorods (AuNRs) are the anisotropic plasmonic nanostructure due to their remarkable optical properties, especially their tunable localized surface plasmon resonance (LSPR). AuNRs have attracted

* Corresponding author.
E-mail address: hoavx@tnus.edu.vn

https//doi.org/10.25073/2588-1124/vnumap.5020

increasing attention in a wide range of applications such as surface-enhanced Raman scattering (SERS) [1], solar harvesting [2], photovoltaics [3], fuel cell [4], sensing [5], photothermal therapy [6], biological imaging [7], drug delivery [8], and so on. Unlike spherical gold nanoparticles, AuNRs exhibit two distinct plasmon bands: a transverse mode around 520 nm and a longitudinal mode in near-infrared (NIR) range. The longitudinal mode can be tuned by adjusting the aspect ratio (length/diameter) of the nanorods [9]. Precise control over the aspect ratio and monodispersity of AuNRs is critical for optimizing their optical and sensing performance. Among the various synthesis strategies, the seed-mediated growth method in the presence of cetyltrimethylammonium bromide (CTAB) has become a widely adopted protocol due to its simplicity and reproducibility [10]. However, CTAB alone often leads to limitations such as broad size distribution, shape impurities (e.g., spheres or cubes), and poor control over aspect ratio in large-scale synthesis [11]. To overcome these drawbacks, binary surfactant system has been introduced, with sodium oleate (NaOL) emerging as a key additive for enhanced anisotropic growth. NaOL acts as a co-surfactant that modifies the micelle environment formed by CTAB, influences the reduction kinetics of gold precursors, and selectively adsorbs on specific crystal facets to direct anisotropic growth [12]. Previous studies have reported that NaOL can improve both the yield and uniformity of AuNRs while providing a pathway for aspect ratio control [13].

Despite its known influence, the detailed correlation between NaOL amount and the optical response of AuNRs, particularly the tunability of the longitudinal LSPR, remains unexplored. Understanding this relationship is essential for rational design of AuNRs with tailored plasmonic properties for specific application, especially the excitation wavelength in SERS or photothermal therapy is critical.

In this work, we systematically investigated the effect of NaOL amount on the morphological and optical characteristics of AuNRs synthesized via the seed-mediated method. By varying NaOL amount, we observed a distinct blue-shift in the longitudinal LSPR, directly correlated with a decrease in aspect ratio, as confirmed by transmission electron microscopy (TEM) images. Our results demonstrate that NaOL enables fine-tuning of LSPR properties through morphological control, providing a simple and scalable strategy for engineering AuNRs with specific optical features.

2. Experimental

2.1. Chemicals

Hydrogen tetrachloroaurate (III) trihydrate ($HAuCl_4.3H_2O$, 99.9%), cetylmethyl ammonium bromide (CTAB, 99%), sodium oleate (NaOL, 97%), silver nitrate ($AgNO_3$, 99%), ascorbic acid (AA, $C_6H_8O_6$, 99%), sodium borohydride ($NaBH_4$, 98%), hydrochloride acid (HCl, 36%) were purchased from Sigma-Aldrich. All chemicals were analytical grade and used as received without further purification. Bidistilled water was used in sample preparation and cleaning glassware.

2.2. Preparation of Au Seeds

A seed solution consisting of tiny spherical gold nanoparticles was prepared as follows: 2.5 ml of 0.2 M CTAB was mixed with 1 ml of 1.25 mM $HAuCl_4$ solution under gentle stirring within 30 minutes. 0.1875 ml of 0.01 M $NaBH_4$ (in ice bath) was rapidly injected to the above mixture so that the molar ratio of $NaBH_4$: $HAuCl_4$ reaches 1.5. After 5-minute stirring, the solution was aged for further 2 hours at room temperature. The solution gradually turned brownish-yellow, indicating the formation of gold seed nanoparticles (Fig. 1a). The reaction equation between $NaBH_4$ and $HAuCl_4$ to create metallic gold is:

$$6NaBH_4 + 2HAuCl_4 \rightarrow 2Au\downarrow + 3H_2\uparrow + 6BH_3 + 6NaCl + 2HCl \quad (1)$$

2.3. Preparation of AuNRs

AuNRs have been prepared from $HAuCl_4$ and ascorbic acid (AA) as follows: 4.5 ml of 0.1 M CTAB was added to 4.5 ml of bidistilled water under gentle stirring within 5 minutes. Then m grams of NaOL (with various amounts of NaOL as indicated in Table 1) was added to the above CTAB solution under continuous stirring for 10 minutes. After that, 0.7 ml of 4 mM $AgNO_3$ solution was gradually injected to the mixture under further stirring for 30 minutes.

Consequently, 0.15 ml of 25 mM $HAuCl_4$ was dropped into the solution under stirring for 1 hour. 0.03 ml of 36% HCl solution was slowly added under stirring for 15 minutes. Finally, 0.034 ml of 0.05 M ascorbic acid (AA) and 0.05 ml of Au seed solution were rapidly injected to the mixture under progressively stirring for 15 seconds. The obtained mixture was aged for 1 hour to form AuNRs (Fig. 1b).

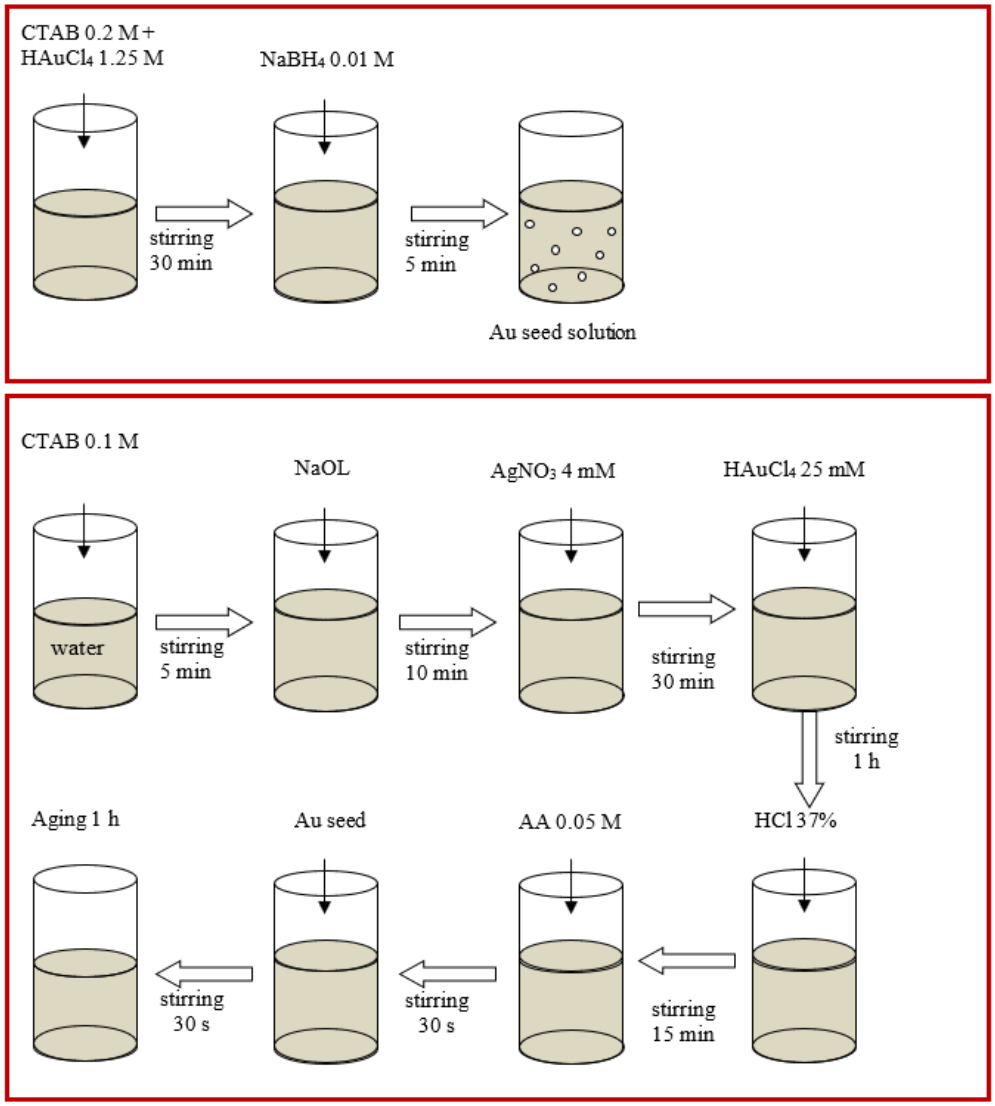

Figure 1. Schematic representation of reduction synthesis of (a) Au seeds, (b) Au nanorods.

The complexation strength of Au(III) with halide ions follows the series $I^- > Br^- > Cl^-$. Therefore, in the presence of CTAB, four Cl^- ligands in $AuCl_4^-$ are replaced by Br^- ions:

$$4CTAB + HAuCl_4 \leftrightarrows 3CTA^+ - Cl^- + CTA^+ - AuBr_4^- + HCl \quad (2)$$

The color of the solution changes from pale-yellow to dark-orange. The $AuBr_4^- - CTA^+$ complex formation will influence their redox potentials and the growth kinetics. Ascorbic acid (AA, $C_6H_8O_6$) reduced Au^{3+} to form metallic Au and dehydroascorbic acid ($C_6H_6O_6$):

$$3C_6H_8O_6 + 2CTA^+ - AuBr_4^+ \rightarrow 2Au\downarrow + 3C_6H_6O_6 + 6HBr + 2CTAB \quad (3)$$

Combining two equations (2) and (3), we have:

$$3C_6H_8O_6 + 2HAuCl_4 + 6CTAB \rightarrow 2Au\downarrow + 3C_6H_6O_6 + 2HCl + 6HBr + 6CTA^+ - Cl^- \quad (4)$$

Au seeds act as catalyst for reducing Au (III) into Au (I):

$$Au^{3+} + 2Au^0 \leftrightarrows 3Au^+ \quad (5)$$

This reaction requires the incorporation of CTAB as following:

$$2CTAB + CTA^+ - AuBr_4^- + 2Au \leftrightarrows 3CTA^+ - AuBr_2^- \quad (6)$$

In the final step, Au (I) is reduced by AA into metallic Au:

$$C_6H_8O_6 + 2CTA^+ - AuBr_2^+ \rightarrow 2Au\downarrow + C_6H_6O_6 + 2HBr + 2CTAB \quad (7)$$

In addition, the reduction potential of AA is lower under acidic condition, so pH value has been applied to modulate Au nanorod growth. HCl was used to low pH value which slow down the growth kinetics, leading to higher aspect ratio. AuNRs are synthesized by growth on CTAB-capped seeds in the presence of silver nitrate. The presence of Ag^+ ions is essential for the synthesis of single-crystal Au nanorods because Ag^+ ions lead to higher selectivity for reduction on the tips and stabilization of lateral facets. The slow reduction helps to achieve a narrower size distribution. The less anisotropic by-product (spheres for single-crystal nanorods) can be separated overnight in a single purification step because the by-product will largely accumulate on a particular area of the grid [14].

The synthesized of nanorods were purified by centrifugation at 9000 rpm for 15 minutes to remove excess surfactants and unreacted precursors. The precipitate was redispersed in bidistilled water to be centrifuged again.

Table 1. Sample labels and amounts of precursors in AuNRs preparation

Sample	NaOL (g)	0.1 M CTAB (ml)	4 mM $AgNO_3$ (ml)	25 mM $HAuCl_4$ (ml)	HCl 36% (ml)	0.05 M AA (ml)	Au seed (ml)
AuNR-NaOL1	0.0061	4.5	0.7	0.15	0.03	0.034	0.05
AuNR-NaOL2	0.0122						
AuNR-NaOL3	0.0244						
AuNR-NaOL4	0.0304						
AuNR-NaOL5	0.0365						
AuNR-NaOL6	0.0487						
AuNR-NaOL7	0.0609						

2.4. Characterization

Field emission scanning electron microscopy images of the samples were obtained using SEM Hitachi S4800 (Japan) operated at 10 kV. The UV-Vis absorption spectra were recorded in Shimadzu UV-2600 spectrophotometer in the range of 400-1250 nm to monitor the longitudinal and transverse resonance peaks. Morphology and size distribution of Au seeds and nanorods were examined using transmission electron microscopy (TEM, JEOL JEM-2100) operated at 120 kV and high-resolution TEM (HRTEM) operated at 200 kV. Based on the TEM images, size distribution of Au seeds was analyzed using ImageJ software. Energy-dispersive X-ray spectroscopy (EDS) was performed on a Hitachi SU 8020 (EDS, Japan) operated at 200 kV. X-ray diffraction (XRD) was performed on a Bruker D8 Advance diffractometer (Germany) with Cu-K_α radiation ($\lambda = 0.154056$ nm) operated at 40 kV to obtain the crystal structure of the samples.

3. Results and Discussion

3.1. Au Seed

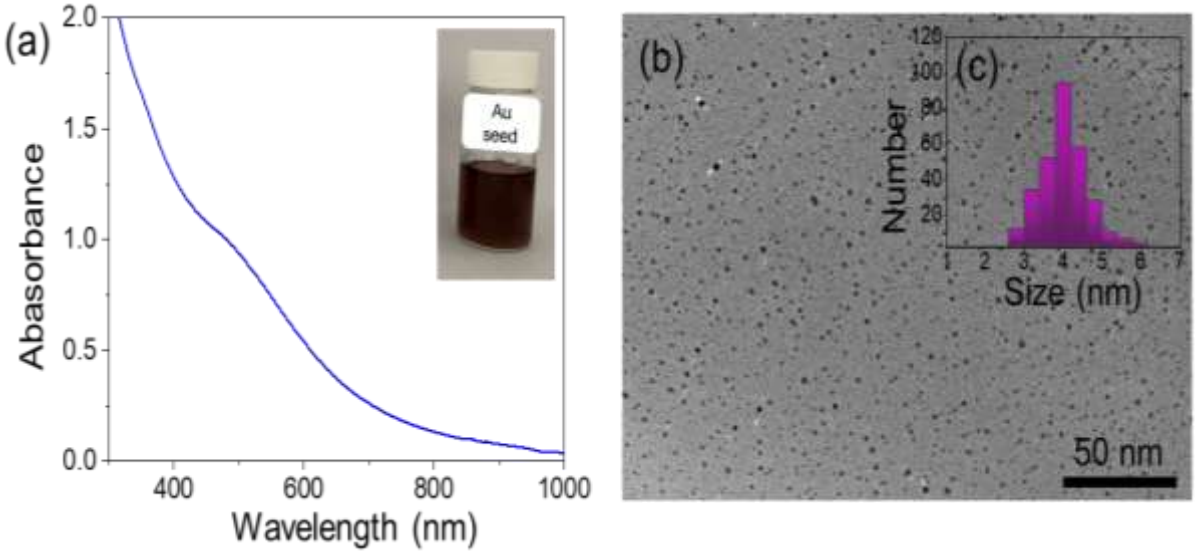

Figure 2. (a) UV-Vis absorption spectrum of Au seeds solution, (inset) picture of the Au seeds solution, (b) TEM image of Au seeds, (c) historgram of size distribution of Au seeds.

Fig. 2a shows the UV-Vis spectrum of Au seeds and their solution appeared light brown (inset). This spectrum did not show any localized surface plasmon resonance (LSPR) band. Fig. 2b shows the TEM image of Au seeds, Fig. 2c shows the histogram of size distribution of Au seeds. It can be seen that the Au seeds are in spherical shape with average size of 4 nm. Au seeds are small nuclei (typically below 5 nm) which serve as the starting point for the development of an anisotropic structure [15]. The monodisperse and same crystallographic seeds is achieved by adding a strong reducing agent such as sodium borohydride under vigorous stirring. The addition of the reductant produces nuclei distributing homogeneously in the entire solution volume. CTAB-capped seeds are used for single-crystal nanorod preparation.

3.2. Effect of NaOL Concentration on LSPR of AuNRs

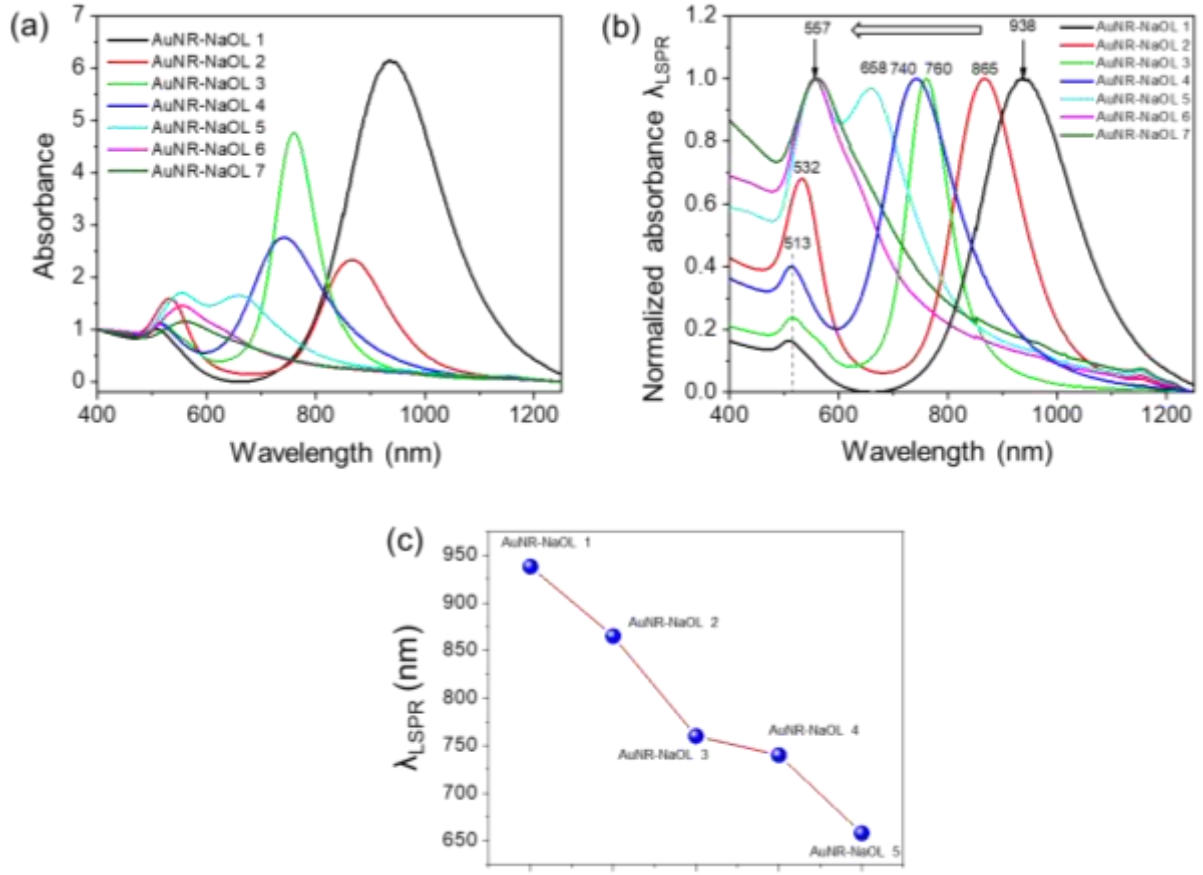

Figure 3. (a) UV-Vis spectra of AuNRs with various amounts of NaOL, (b) the normalized corresponding absorbance spectra, (c) the longitudinal peak position as a function of NaOL amount.

UV-Vis-NIR spectra provide a wealth of information. The high aspect ratio of AuNRs gives the longitudinal plasmon band in the near infrared (NIR) range. This longitudinal band can be tuned from the NIR into the visible range using sodium oleate. Increasing sodium oleate (NaOL) amount from 6.1 mg to 60.9 mg led to the blue-shift of the longitudinal localized plasmon resonance (LSPR) peak from 938 nm (AuNR-NaOL1) to 557 nm (AuNR-NaOL7) (Fig. 3). This shift indicated the reduction of the nanorod aspect ratio and implicated the role of NaOL in the nanorod growth process. In addition, the LSPR absorbance decreased as the NaOL amount increased, except for AuNR-NaOL3 sample. The ratio between the maximum absorbance of the longitudinal (LSPR) and transverse (TSPR) bands is OD_{LSPR} / OD_{TSPR}. The AuNR-NaOL3 sample exhibited $\lambda_{LSPR} = 760$ nm and $OD_{LSPR} / OD_{TSPR} = 4.2$ larger than that of AuNR-NaOL2 ($OD_{LSPR} / OD_{TSPR} = 1.47$) (Table 2). The AuNR-NaOL4 sample exhibited $\lambda_{LSPR} = 742$ nm and $OD_{LSPR} / OD_{TSPR} = 2.5$. In contrast, the AuNR-NaOL5 exhibited $OD_{LSPR} / OD_{TSPR} = 0.97 < 1$. AuNR-NaOL6 and AuNR-NaOL7 exhibited only one peak at 555 and 561 nm, respectively, and unsymmetrical spectra.

The blue-shift of the longitudinal plasmon band is observed during growth, suggesting a gradual decrease in aspect ratio of nanorods throughout the growth process. The higher NaOL amount may

restrict longitudinal growth by steric hindrance in respect of gold ion accessibility to the $\{111\}$ facets. Additionally, NaOL can accelerate gold ion reduction that can lead to less anisotropic elongation, resulting in shorter rods and a blueshift. On the other hand, NaOL can passivate the lateral facet, inhibit tip growth, resulting in a lower aspect ratio. Ye et al., [12] observed that excess NaOL can suppress longitudinal growth due to overly stabilized CTAB/NaOL bilayers. Similarly, Zürbes et al., [16] noted that modifying surfactant ratios can flip the growth dynamics from elongation to lateral expansion. The full width at half maximum (FWHM) and the shape of the longitudinal LSPR band give us the size dispersion, while the plasmon band position gives us the average aspect ratio. To better understand the origin of the observed blue-shift in the localized surface plasmon resonance (LSPR) with increasing NaOL concentration, we distinguish between two key mechanisms: i) Inhibition of longitudinal growth; and ii) Enhancement of lateral growth. Both mechanisms result in a decrease in particle aspect ratio, yet through distinct morphological pathways. To elucidate their relative contributions, we analyzed the aspect ratio distribution (Fig. 4) of nanoparticles from TEM images, alongside the spectral full width at half maximum (FWHM) of the LSPR peaks. As shown in Fig. 4 (a-d), increasing NaOL concentration results in a marked reduction in the mean aspect ratio of particles, from 20 to 1.2, accompanied by an increase in circularity, indicative of more spherical-like morphologies. This trend suggests a progressive enhancement of lateral growth. Simultaneously, the FWHM of the LSPR peak decreases from 201 nm to 60 nm corresponding to AuNR-NaOL1 and AuNR-NaOL6, reflecting a change in size and shape distribution and possibly a reduction in damping effects due to increased monodispersity. The combination of these trends indicates that both mechanisms are at play, but enhancement of lateral growth becomes increasingly dominant at higher NaOL concentrations.

Table 2. The optical density (OD) and the peak wavelength of two modes: longitudinal and transverse, in the UV-Vis absorption spectra

Sample	TSPR		LSPR		OD_2/OD_1
	OD_1	λ_1	OD_2	λ_2	
AuNR-NaOL1	1.00684	508	6.14175	936	6.10
AuNR-NaOL2	1.588	532	2.332	867	1.47
AuNR-NaOL3	1.132	514	4.757	760	4.20
AuNR-NaOL4	1.104	514	2.757	742	2.50
AuNR-NaOL5	1.7	554	1.646	659	0.97
AuNR-NaOL6	1.451	555	-	-	-
AuNR-NaOL7	1.152	561	-	-	-

TEM images show the length, thickness, aspect ratio of nanorods and sample size dispersion. It can also be used to asscess the presence or absence of by-products. Figure 4a show TEM image of AuNR-NaOL1 sample with the length of ~ 60 nm and the diameter of ~ 3 nm. Figure 4b shows TEM image of AuNR-NaOL2 sample with the length of ~ 45 nm and diameter of ~ 8 nm. The appearance of spherical shape exhibited the rod formation efficiency decreased. The nanorod diameter increased, or length/diameter ratio decreased, as the NaOL amount increased. This result agrees with the previous publication [11]. TEM image of AuNR-NaOL3 as shown in Figure 4c exhibites the length of ~ 65 nm and the diameter of ~ 16 nm. Gold nanospheres transform into perfect nanorods, that can explain the blue shift of the longitudinal plasmon band [17]. AuNR-NaOL5 exhibites the spherical morphology with average diameter of ~ 85 nm (Fig. 4d). AuNR-NaOL6 and AuNR-NaOL7 show the ununiform spherical morphology (Fig. 4e). The reduction takes place predominantly on the rod tips with the highest surface energy, so the freshly reduced Au atoms form the most thermodynamically stable crystallographic habit. A certain amount of by-products with different shapes is always present along with AuNRs.

The stabilization of crystallographic facets is under thermodynamic control, while the anisotropic growth of nanorods is under kinetic control. AuNRs synthesis requires both thermodynamic and kinetic controls which significantly increase the number of parameters such as length, diameter, aspect ratio, reduction yield and shape yield. In the seed growth protocol, nucleation is performed to prepare the seeds which are subsequently added to the growth solution for nanorod production [18]. A strong reduction agent, sodium borohydride, leads to the formation of Au seeds through the reduction of $HAuCl_4$ salt precursor into metallic Au. CTAB is a suitable surfactant for the synthesis of AuNRs stems from its phase behavior. CTAB forms rod-shaped micelles to induce anisotropic growth on spherical seeds [19]. CTAB acted as a face-specific capping agent, in which the bromide counterion has a more important role in the anisotropic growth than the surfactant itself [20]. The growth of AuNRs is characterized by a slow kinetics which needs an hour to complete nanorod growth.

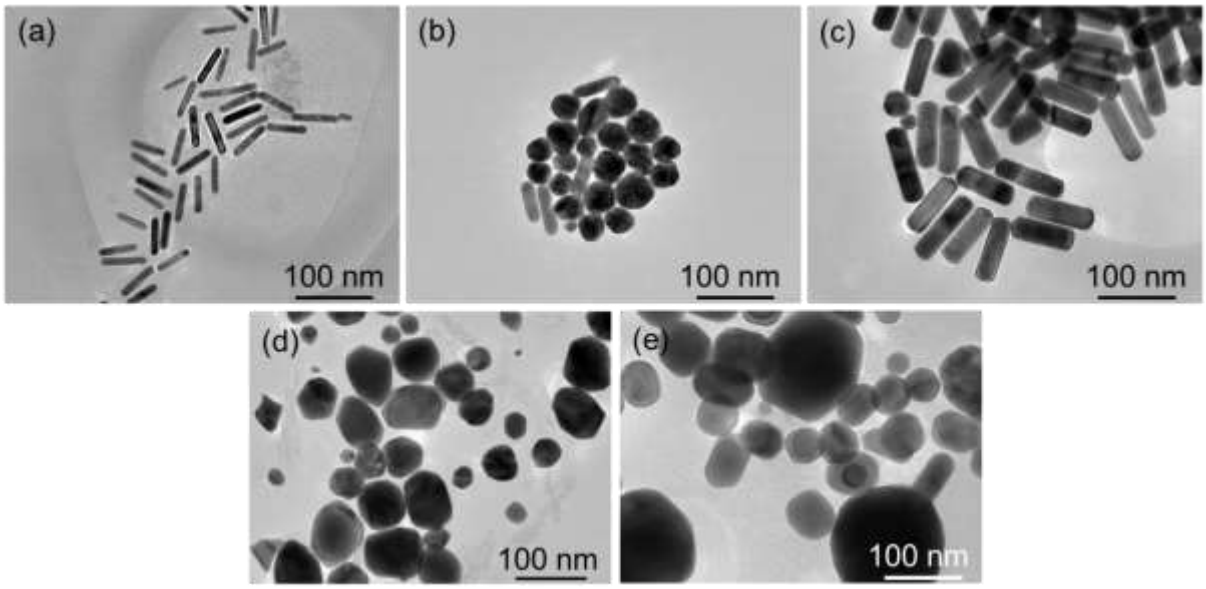

Figure 4. TEM images of (a) AuNR-NaOL1, (b) AuNR-NaOL2, (c), AuNR-NaOL3, (d) AuNR-NaOL5, (e) AuNR-NaOL6.

3.3. XRD, HRTEM, and EDS Results

XRD patterns of Au seeds and AuNR-NaOL3 samples have 4 diffraction peaks at $2\theta = 37.9°$, 44.2°, 64.4°, and 76.9°, corresponding to (111), (200), (220), and (311) crystal planes (JCPDS card number 08-0234) [21] (Fig. 5a). XRD results confirmed the high crystallinity of the obtained products. No other peaks are observed, that exhibits the purity of the obtained samples. Fig. 5b shows the crystallite sizes of Au seeds and AuNR-NaOL3 calculated from four main diffraction peaks of (111), (200), (220), and (311) using Scherrer equation [22]:

$$D = \frac{k\lambda}{\beta \cos\theta} \tag{8}$$

where D is the crystallite size, $k = 0.893$ is the Scherrer constant, $\lambda = 0.154056\,\text{nm}$ is the X-ray wavelength, β is the half-bandwidth of the X-ray spectral peak (in radian), θ is the Bragg diffraction angle (in degree).

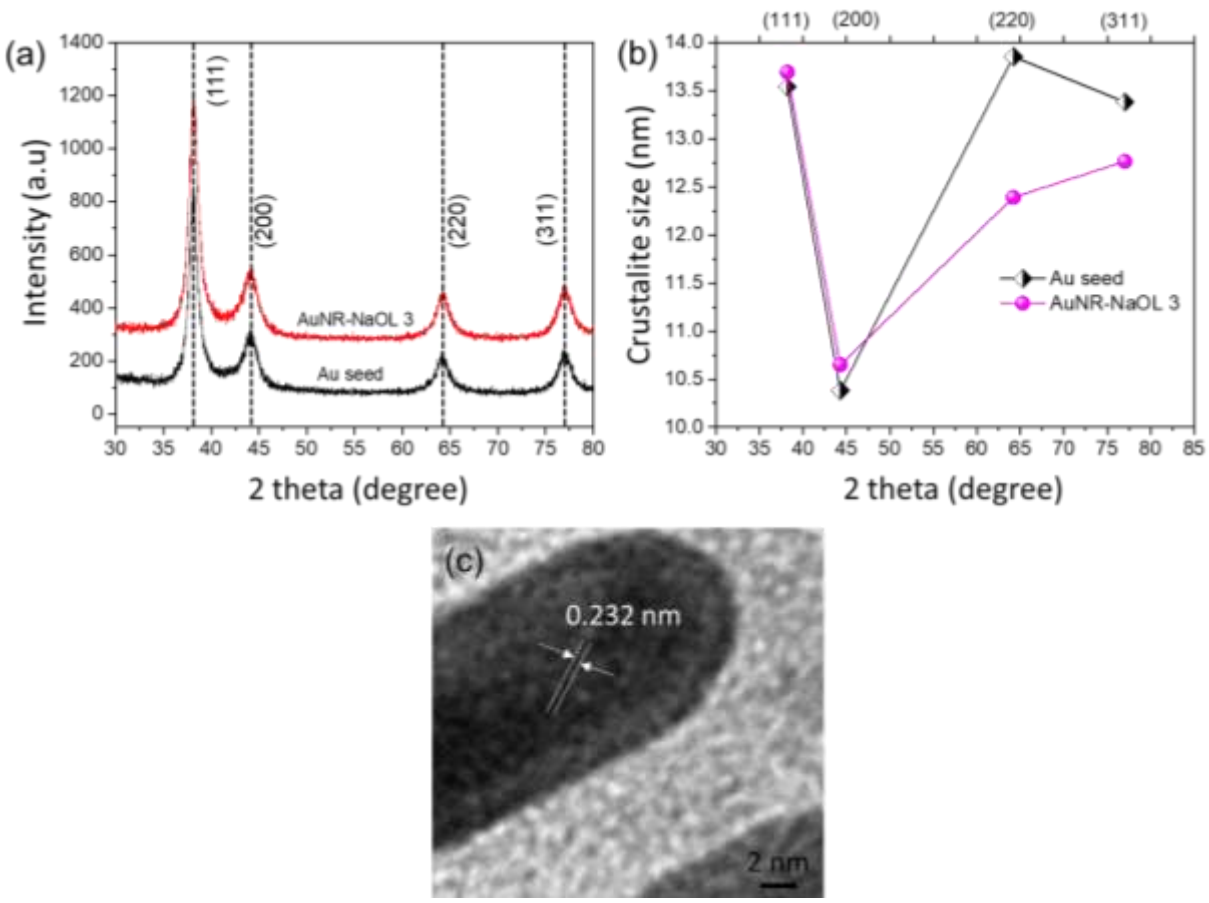

Figure 5. (a) XRD patterns of Au seeds, AuNR-NaOL3 samples, (b) crystallite sizes of Au seeds, AuNR-NaOL3 samples calculated from four main diffraction peaks of (111), (200), (220), and (311) using Scherrer equation, (c) HRTEM image of AuNR-NaOL3 sample.

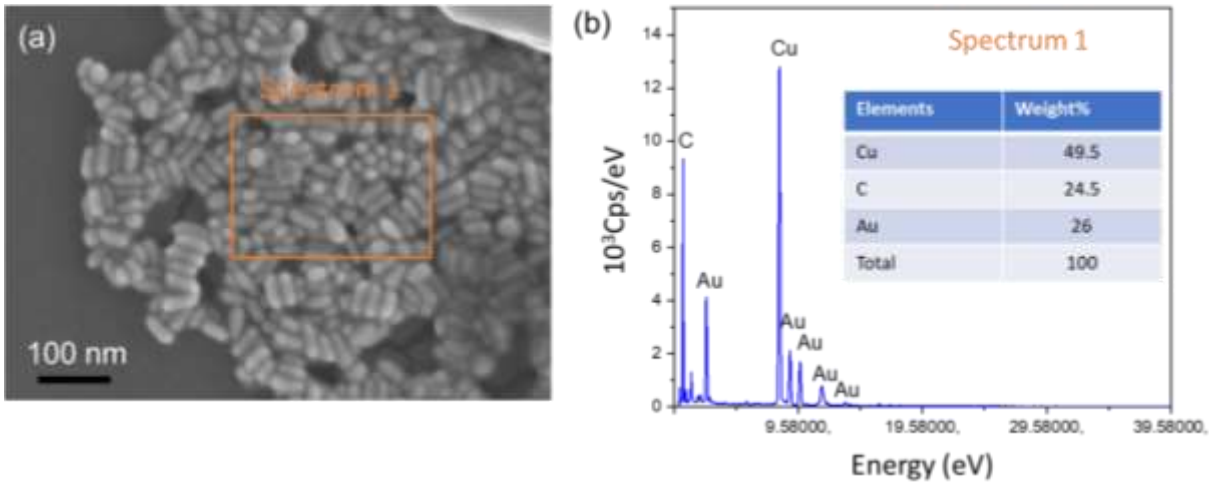

Figure 6. (a) SEM image, (b) EDS spectrum of AuNR-NaOL3 sample.

Fig. 5c shows the HRTEM image of an individual AuNR-NaOL3 nanorod, where the interplanar (111) lattice spacing is measured to be around 0.232 nm, typical for cubic gold.

Fig. 6a presents the SEM image of AuNR-NaOL3 sample. AuNRs are clearly visible, illustrating that AuNRs were successfully fabricated. The length and diameter of the AuNRs were measured around 65 nm and 16 nm, respectively. The energy-dispersive X-ray spectroscopy (EDS) chart measured at AuNRs and the corresponding element ratio table are displayed in the Fig. 6b.

4. Conclusion

Our findings demonstrate that sodium oleate (NaOL) is essential for controlling gold nanorod morphology. By controlling NaOL amount lead to blue-shift of the longitudinal localized plasmon resonance (LSPR) peak from 938 nm to 557 nm. However, excess NaOL can suppress longitudinal growth, leading to AuNRs with low aspect ratio and blue-shifted LSPR. This research implicates that the surfactant can be used to obtain the desired morphology and plasmonic behavior of gold as well as other metals.

Acknowledgement

The authors are grateful to Vietnam Ministry of Science and Technology for the financial support of ĐT CTVL 2021-2025 under grant number ĐTĐLCN.23/23.

References

[1] W. Lu, Y. Jiang, X. Yao, Y. Yu, W. Shen, M. Yang, X. Huang, X. Tang, Dispersive Pd Islands-Deposited Au Nanorods for in Situ SERS Monitoring of Catalytic Reaction, RSC Advances, Vol. 15, 2025, pp. 6663-6667, https://doi.org/10.1039/D5RA01059D.

[2] D. J. D. Aberasturi, A. B. S. Montes, L. M. L. Marzán, Modern Applications of Plasmonic Nanoparticles: from Energy to Health, Advanced Optical Materials, Vol. 3, 2015, pp. 602-617, https://doi.org/10.1002/adom.201500053.

[3] R. C. Wadams, C. W. Yen, D. P. Butcher Jr, H. Koerner, M. F. Durstock, L. Fabris, C. E. Tabor, Gold Nanorod Enhanced Organic Photovoltaics: The Importance of Morphology Effects, Organic Electronics, Vol. 15, 2014, pp. 1448-1457, https://doi.org/10.1016/j.orgel.2014.03.039.

[4] Y. C. Ting, Y. T. Lin, G. J. Wang, A Novel Anode of Gold Nanoparticle Coated Au Nanorod Arrays for Nonenzymatic Glucose Fuel Cells, Journal of Power Sources, Vol. 590, 2024, pp. 233792, https://doi.org/10.1016/j.jpowsour.2023.233792.

[5] L. N. Meng, J. Zhu, G. J. Weng, J. J. Li, J. W. Zhao, Optimization of the Ultra-Narrow Plasmonic Bandwidth of Pt-Coated Au Nanorod: The Application in Refractive Index Sensing, Physica E: Low-dimensional Systems and Nanostructures, Vol. 135, 2022, pp. 114996, https://doi.org/10.1016/j.physe.2021.114996.

[6] J. He, H. Zhang, J. Zhu, X. Zhang, X. Liu, K. Ramachandraiah, F. Ke, Layer-by-Layer Synthesis of Au Nanorods@ Metal-Organic Framework Core-Shell Nanohybrids for Magnetic Resonance Imaging Guided Photothermal Therapy, Materials Today Communications, Vol. 33, 2022, pp. 104560, https://doi.org/10.1016/j.mtcomm.2022.104560.

[7] Z. Ma, H. Xia, Y. Liu, B. Liu, W. Chen, Y. Zhao, Applications of Gold Nanorods in Biomedical Imaging and Related Fields, Chinese Science Bulletin, Vol. 58, 2013, pp. 2530-2536, https://doi.org/10.1007/s11434-013-5720-7.

[8] S. Hajebi, M. Chamanara, S. S. Nasiri, M. Ghasri, A. Mouraki, R. Heidari, A. Nourmohammadi, Advances in Stimuli-Responsive Gold Nanorods for Drug-Delivery and Targeted Therapy Systems, Biomedicine & Pharmacotherapy, Vol. 180, 2024, pp. 117493, https://doi.org/10.1016/j.biopha.2024.117493.

[9] M. Gorbunova, V. Apyari, S. Dmitrienko, Y. Zolotov, Gold Nanorods and Their Nanocomposites: Synthesis and Recent Applications in Analytical Chemistry, TrAC Trends in Analytical Chemistry, Vol. 130, 2020, pp. 115974, https://doi.org/10.1016/j.trac.2020.115974.

[10] Q. Li, T. Bürgi, H. Chen, Preparation of Gold Nanorods of High Quality and High Aspect Ratio, Journal of Wuhan University of Technology, Vol. 25, 2010, pp. 104-107, https://doi.org/10.1007/s11595-010-1104-x.

[11] L. Scarabelli, A. S. Iglesias, J. P. Juste, L. M. L. Marzán, A Tips and Tricks Practical Guide to The Synthesis of Gold Nanorods, The Journal of Physical Chemistry Letters, Vol. 6, 2015, pp. 4270-4279, https://doi.org/10.1021/acs.jpclett.5b02123.

[12] X. Ye, C. Zheng, J. Chen, Y. Gao, C. B. Murray, Using Binary Surfactant Mixtures to Simultaneously Improve The Dimensional Tunability and Monodispersity in the Seeded Growth of Gold Nanorods, Nano Letters, Vol. 13, 2013, pp. 765-771, https://doi.org/10.1021/nl304478h.

[13] A. K. Sahu, A. Das, A. Ghosh, S. Raj, Understanding Blue Shift of the Longitudinal Surface Plasmon Resonance During Growth of Gold Nanorods, Nano Express, Vol. 2, 2021, pp. 010009, https://doi.org/10.1088/2632-959X/abd966.

[14] A. S. Iglesias, M. Grzelczak, J. P. Juste, L. M. L. Marzán, Binary Self-Assembly of Gold Nanowires with Nanospheres and Nanorods, Angewandte Chemie International Edition, Vol. 122, 2010, pp. 10181-10185, https://doi.org/10.1002/anie.201005891.

[15] A. Gole, C. J. Murphy, Seed-Mediated Synthesis of Gold Nanorods: Role of the Size and Nature of the Seed, Chemistry of Materials, Vol. 16, 2004, pp. 3633-3640, https://doi.org/10.1021/cm0492336.

[16] K. R. Zürbes, E. Mani, S. Bandyopadhyay, Synthesis of Anisotropic Gold Nanoparticles in Binary Surfactant Mixtures: A Review on Mechanisms of Particle Formation, RSC Advances, Vol. 15, 2025, pp. 4377-4407, https://doi.org/10.1039/D4RA06358A.

[17] B. M. Kim, S. H. Seo, A. Joe, K. D. Shim, E. S. Jang, Growth Mechanism of Gold Nanorods in Binary Surfactant System, Bulletin of the Korean Chemical Society, Vol. 37, 2016, pp. 931-937, https://doi.org/10.1002/bkcs.10805.

[18] B. Nikoobakht, M. A. E. Sayed, Preparation and Growth Mechanism of Gold Nanorods (NRs) Using Seed-Mediated Growth Method, Chemistry of Materials, Vol. 15, 2003, pp. 1957-1962, https://doi.org/10.1021/cm020732l.

[19] C. J. Murphy, L. B. Thompson, D. J. Chernak, J. A. Yang, S. T. Sivapalan, S. P. Boulos, J. Huang, A. M. Alkilany, P. N. Sisco, Gold Nanorod Crystal Growth: From Seed-Mediated Synthesis to Nanoscale Sculpting, Current Opinion in Colloid & Interface Science, Vol. 16, 2011, pp. 128-134, https://doi.org/10.1016/j.cocis.2011.01.001.

[20] J. Gao, C. M. Bender, C. J. Murphy, Dependence of the Gold Nanorod Aspect Ratio on yhe Nature of the Directing Surfactant in Aqueous Solution, Langmuir, Vol. 19, 2003, pp. 9065-9070, https://doi.org/10.1021/la034919i.

[21] H. Du, F. Wang, R. Zhang, Y. Jing, Y. Chang, L. Wang, T. Zhou, X. Wang, G. Zhang, Z. Zhang, Rolling Circle Amplification-Induced Self-Assembly of Gold Nanorods to form One-Dimensional Arrays Equipped 'Multi-Locator'for Fluorescence Imaging and Enhancement Photothermal Tumor Therapy, Journal of Molecular Liquids, Vol. 426, 2025, pp. 127317, https://doi.org/10.1016/j.molliq.2025.127317.

[22] B. D. Cullity, S.R. Stock, Elements of X-Ray Diffraction, 3rd Ed., Prentice-Hall Inc., ISBN 0-201-61091-4, 2001, pp. 96-102.